Expansion of operating frequencies for Radio Frequency Modulation Calorimetry

A Major Qualifying Project Report:

Submitted to the Faculty

of the

Worcester Polytechnic Institute

in partial fulfillment of the requirements for the

Degree of Bachelor of Science

by

_____

Brenden C. Brown

Date: April 26, 2007

Approved:

_____

Professor Germano Iannacchionne

Abstract:

The goal of this project was to make improvements to an original RF calorimeter designed by Saimir Barjami for his doctoral dissertation, by increasing the range of available operating frequencies. This project increased the frequencies available through additional matching networks, and simulated results of several possible experiments. These simulations were provided through an original tool allowing adjustment of all relevant variables to predict the behavior of a variety of samples in any similar RF calorimeter.

Table of Contents

List of Figures

List of Tables

Chapter 1: Introduction

New compounds and materials such as liquid crystals are constantly being developed and researched. One component in the body of knowledge of a material is its thermodynamic properties. In order to research phase transitions and heat capacity, a technique known as calorimetry is used. Calorimetry involves the use of controlled heating of a sample to study the changes in its physical properties as the temperature is varied. There are several methods used, such as Adiabatic Calorimetry, Differential Scanning Calorimetry, and Adiabatic Scanning Calorimetry. In the late 1960s, a technique known as Modulation Calorimetry (MC) was introduced, which has become a powerful technique for the study of phase transitions in liquid crystals.

The MC technique involves the use of applying periodically moderated sinusoidal power to a small sample, and measuring the resulting temperature response. The amplitude of this temperature response is inversely proportional to the heat capacity of the sample. The applied power is historically provided through Joule or resistive heating, where a sinusoidal AC current is passed through a resistive element that is in contact with the sample, and the temperature response is measured through a thermometer that is also attached to the sample. The AC/MC method of calorimetry has many advantages over other methods of determining heat capacity, such as only requiring a small sample size, running under near equilibrium conditions, and not needing thermal isolation, such as is required in adiabatic calorimetry. However, the use of Joule heating is not without disadvantages.

When using Joule heating, only the portion of the sample in contact with the heater is immediately heated. This leads to a temperature gradient across the sample, with the portion in contact with the heater at the highest temperature, and the portion furthest at the lowest temperature. This temperature gradient is unwanted, and limits the frequencies that can be used for the heating and cooling cycle, because higher frequencies result in a larger gradient.

A new technique known as Radio Frequency Modulation Calorimetry has been developed recently, which uses a different method of heating than Joule heating. When using RF heating, the sample is used as a dielectric in a capacitor, which is subjected to a

sinusoidal alternating voltage. This high frequency electromagnetic field causes polar molecules in the sample to rotate rapidly, which through friction causes the sample to heat uniformly. This eliminates temperature gradients across the sample, and allows for a wider range of modulating frequencies to be used.

In this work we describe improvements made to an existing RF/MC calorimeter, which allow for a wider range of heating frequencies. In order for the calorimeter to absorb as much of the transmitted power as possible, an LC matching network is placed between the power source and the calorimeter, which is specific to a single operating frequency. The math is developed to provide a computer simulation of the heating power at frequencies near resonance, for any desired resonant frequency.

Chapter 2: Theory

In this chapter, the theory essential for understanding the operation of the RF/MC calorimeter is described. Capacitive heating is explained to show how the sample is heated. Traditional AC/MC theory is used to show how the thermometer design allows for the relevant measurements. Finally, the design of the RF/MC calorimeter is described, as well as the electronic control program.

Theory of capacitive heating

The heating power is produced because the sample is not a perfect dielectric, but is "lossy." When the electric field is flipped back and forth at a high frequency, polar molecules must rapidly rotate to realign themselves in the changing field. This rotation causes a heating effect similar to friction. In a circuit with pure capacitance, the current leads the applied voltage by $\pi/2$. Because the dielectric is lossy, the capacitance is imperfect, and the current will lead the voltage by less than $\pi/2$. The angle between pure capacitance with a $\pi/2$ lead and the phase shift of the actual circuit is known as the angle δ, and the phase shift is θ.

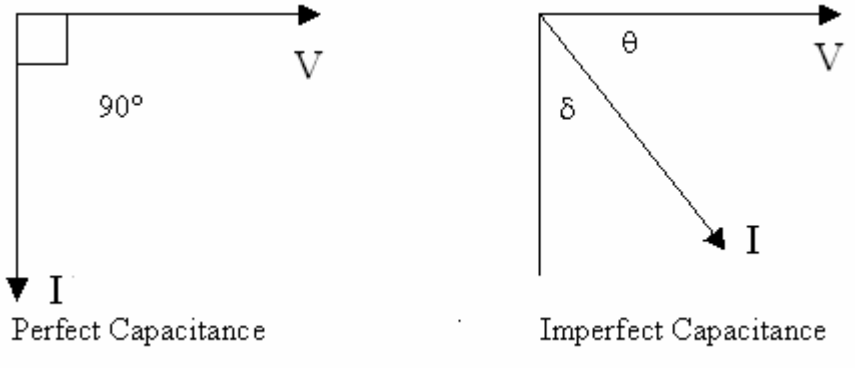

Figure 2-1: Current-Voltage relations in perfect and imperfect capacitance

Current through a resistance is in phase with the voltage, and as discussed above, current through a capacitive element leads the voltage by $\pi/2$. The current in the above diagram can be resolved into two currents, one in phase with the voltage, and one $\pi/2$ out of phase. This is equivalent to a circuit with a capacitance and resistance in parallel.

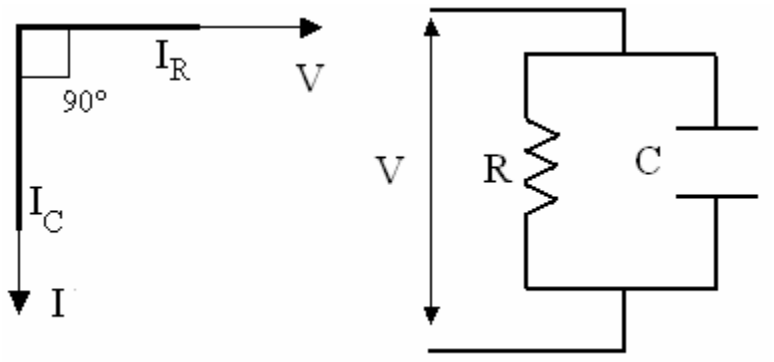

Figure 2-2: Resolving imperfect capacitance into a virtual resistance and capacitance

In this circuit, R is the equivalent resistance due to the imperfect dielectric, C is the value of the capacitance, I_R is the current through the resistance, and I_C is the current through the capacitance. Using this terminology, the following equations can be written:

2.1 $$I_R = I\sin(\delta) \qquad I_C = I\cos(\delta)$$

2.2 $$X_C = \frac{1}{2\pi fC} \qquad I_C = \frac{V}{X_C} = 2\pi fcv$$

These equations can be used to calculate the power absorbed by the dielectric, through the use of the loss factor tan δ:

2.3 $$\tan\delta = \frac{I_R}{I_C} = \frac{V/R}{2\pi fCV} = \frac{1}{2\pi fCR}$$

From this, the equivalent resistance R can be expressed in terms of f, C, and tan δ:

2.4 $$R = \frac{1}{2\pi fC\tan(\delta)}$$

Now we can calculate the power absorbed:

2.5 $$P = \frac{V^2}{R} = 2\pi fC\tan(\delta)V^2$$

This power is what is absorbed by the sample, and is dependent upon the driving frequency, the capacitance, the loss factor, and the voltage. The frequency is adjustable, the loss factor is a physical constant, and the voltage is fixed. The capacitance depends upon the geometry of the capacitor and upon the dielectric constant ε of the sample. For a parallel plate capacitor, the capacitance is given by:

2.6 $$C = \frac{A|\varepsilon|}{d}$$

Inserting Eq 2.6 into Eq 2.5 gives:

2.7 $$P = 2\pi f C \tan(\delta) V^2 = \omega_d \frac{A}{d} \tan(\delta) |\varepsilon| V^2$$

Where ω_d is the angular driving frequency, $\omega=2\pi f$. This equation represents the power absorbed by a lossy dielectric in a parallel plate capacitor with an applied voltage V being driven at a frequency ω_d. In the actual circuit, which can be modeled as an LRC oscillator as shown in Figure 2-3, the voltage across the capacitor is not necessarily the same as the voltage of the driving frequency, as we shall show. Due to resonance effects, the the voltage across the capacitor can be increased or decreased, depending on how close the driving frequency is to the resonant frequency.

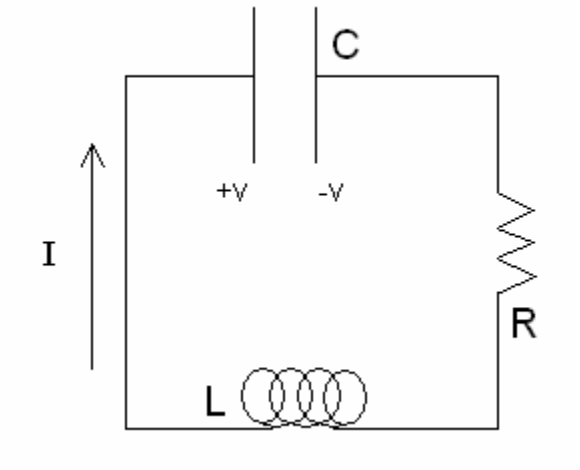

Figure 2-3: an LCR circuit

To determine the voltage across the capacitor, the circuit can be analyzed using Kirchoff's voltage and current laws. The net voltage is zero:

2.8 $$V_0 \cos(\omega t) - iR - \frac{q}{C} - L\frac{di}{dt} = 0$$

Replacing i with dq/dt and rearranging gives:

2.9 $$\frac{V_0}{L}\cos(\omega t) = \frac{d^2 q}{dt^2} + \frac{dq}{dt}\frac{R}{L} + \frac{q}{LC}$$

Defining $\frac{1}{LC}$ as ω_0^2 and $\frac{R}{L}$ as γ gives

2.10 $$\frac{V_0}{L}\cos(\omega t) = \frac{d^2 q}{dt^2} + \gamma\frac{dq}{dt} + \omega_0^2 q$$

Changing to a complex exponential, a solution can be assumed to be of the form:

2.11 $$q = \mathrm{Re}\left[Ae^{j(\omega t-\delta)}\right]$$

Where A is in Coulombs. This is solved to give:

2.12 $$\left(\omega_0{}^2 - \omega^2\right)A + j\gamma\omega A = \frac{V_0}{L}e^{j\delta}$$

This is equivalent to vector addition, where two orthogonal vectors are combined to form another vector, forming a triangle. Through some trigonometric manipulation, this gives:

2.13 $$A = \frac{V_0/L}{\left(\left(\omega_0{}^2 - \omega^2\right)^2 + (\gamma\omega)^2\right)^{1/2}}$$

Multiplying by $L\omega_0{}^2$ gives

2.14 $$AL\omega_0{}^2 = \frac{V_0}{\left(\left(1-\left(\frac{\omega}{\omega_0}\right)^2\right)^2 + \left(\frac{\gamma\omega}{\omega_0{}^2}\right)^2\right)^{1/2}}$$

Assigning $Q = \frac{\omega_0{}^2}{\gamma}$ as the quality factor, and noticing that the unit Coulombs * Henrys / s^2 are the same unit as Volts, we finally have:

2.15 $$V = \frac{V_0}{\left(\left(1-\left(\frac{\omega}{\omega_0}\right)^2\right)^2 + \left(\frac{\omega}{Q\omega_0}\right)^2\right)^{1/2}}$$

Using this voltage in the equation Eq 2.7 gives:

2.16 $$P = \frac{A}{d}\omega_d \tan(\delta)|\varepsilon| \frac{V_0{}^2}{\left(\left(1-\left(\frac{\omega_d}{\omega_0}\right)^2\right)^2 + \left(\frac{\omega_d}{Q\omega_0}\right)^2\right)}$$

From this equation, it is apparent that the power delivered to the sample depends upon the driving frequency, voltage, loss factor, permittivity, and the physical shape of the capacitor and the quality and resonance of the circuit.

Review of MC Calorimetry

In all MC calorimeters, heat capacity is measured by periodically heating the sample. This results in an oscillating temperature, where the amplitude is related to the

heat capacity of the cell and sample. Heat capacity is defined as the amount of energy needed to raise 1 gram of a material by 1 Kelvin. MC Calorimetry has many advantages over other techniques for measuring the heat capacity. All measurements are taken under near equilibrium conditions, which is important because all thermodynamic theory of phase transitions is based upon equilibrium conditions. Due to computer automation, relative resolutions can reach 0.06%, and can achieve very high caloric sensitivity with samples as small as 10-20ml. This helps ensure thermal equilibrium throughout the sample, and large quantities of samples are not always accessible. Finally, thermal isolation is not required, unlike in adiabatic calorimetry.

The derivation of the heat capacity calculations is based on a thermal model of the system, which under certain conditions is geometry independent. The one-lump thermal model shown in Figure 2-4 consists of a number of elements: a cell heater with heat capacity C_h and thermal conductance K_h, a thermometer with heat capacity C_θ and thermal conductance K_θ, a sample with heat capacity C_s and thermal conductance K_s, and the cell itself, with heat capacity C_c. The cell is also linked to a controlled bath at temperature T_b through a thermal conductance K_b.

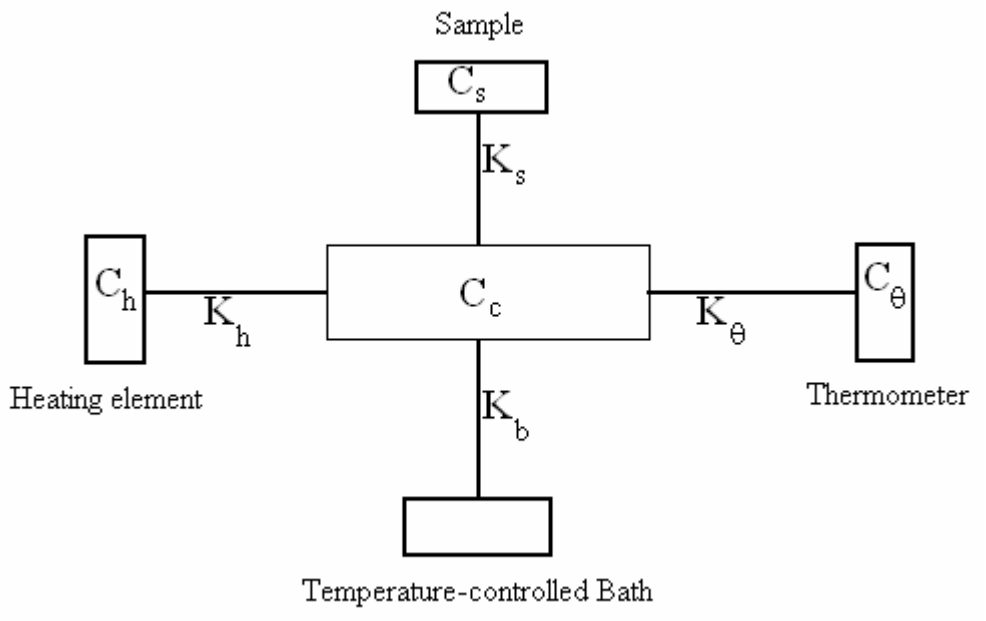

Figure 2-4: Thermal model for AC Calorimetry

Using this model, the total heat capacity is equal to the sum of the various heat capacities:

2.17 $$C = C_h + C_\theta + C_s + C_c$$

The thermal relaxation time constant is the time for the temperature to drop to $1\text{-}e^{-1}$, or by 63%, and is equal to the ratio of the heat constant divided by the thermal conductance:

2.18 $$\tau_\theta = \frac{C_\theta}{K_\theta}, \qquad \tau_h = \frac{C_h}{K_h}, \qquad \tau_s = \frac{C_s}{K_s}$$

The external and internal relaxation times are defined as:

2.19 $$\tau_e = \frac{C}{K_b}, \text{ external;} \qquad \tau_i^{\,2} = \tau_\theta^{\,2} + \tau_h^{\,2} + \tau_s^{\,2}, \text{ internal}$$

The external time constant is related to the time for the entire system to reach thermal equilibrium with the bath. The internal time constant represents the time needed for the system to reach an equilibrium with the applied heat. This heat is traditionally supplied by running current through a resistive wire in thermal contact with the cell. This is done through applying a sinusoidally modulated voltage, which radiates power:

2.20 $$P = \frac{V^2}{R} = \frac{V_0^{\,2}\cos^2(\omega_v t)}{R}$$

This supplies a heat of:

2.21 $$\dot{Q} = \dot{Q}_0 \cos^2(\omega_v t) = \tfrac{1}{2}\dot{Q}_0\left(1 + \cos(2\omega t)\right)$$

Where $2\omega_v t$ is the angular heating frequency, which is twice the voltage frequency. This equation has both a constant term and a time-dependent oscillating term. The amplitude of these oscillations is given by:

2.22 $$T_{ac} = \frac{\dot{Q}_0}{2\omega c}\left(1 + \frac{1}{(\omega\tau_e)^2} + \omega^2\left(\tau_\theta^{\,2} + \tau_h^{\,2} + \tau_s^{\,2}\right)\right)^{-1/2}$$

And the phase shift will be:

2.23 $$\alpha = -\frac{\pi}{2} + \arctan\left(\frac{1}{\omega\tau_e} - \omega\tau_i^{\,*}\right)$$

where $\tau_i^{\,*} = \tau_h + \tau_s + \tau_\theta$ is the time constant.

Eq 2.22 is the exact solution for the temperature oscillations, but a close approximation can be made if the frequency is between the inverses of the external and internal time constants:

2.24 $$\frac{1}{\tau_e} < \omega < \frac{1}{\tau i}$$

Then T_ac can be approximated as:

2.25 $$T_{ac} \cong \frac{\dot{Q}_o}{2\omega C}$$

And the total heat capacity can be simplified to:

2.26 $$C \approx C^* \equiv \frac{\dot{Q}_0}{2\omega T_{ac}}$$

If the conditions in Eq 2.24 are satisfied, we can use this approximation for the total heat capacity. These conditions can be fulfilled by adjusting the external and internal time constants. The external time constant can be chosen through proper selections for the material, length and cross-sectional area of the electrical leads for the heater and thermometer. For the internal time constant, the time constants of the thermometer and heater are generally short enough to be temperature independent, so the sample thickness is the relevant variable. If the sample thickness is less than the thermal diffusion length, then the system is geometry independent, and the locations of the heater and thermometer are not relevant:

2.27 $$l = \left(\frac{2K_s A}{\omega C_s} \right)^{1/2}$$

Where A is the cross sectional area of the sample. If the thickness of the sample exceeds the thermal diffusion length, then the sample will not reach equilibrium with the applied heat, and the temperature oscillations will not happen as analyzed. For the current calorimeter, Dr Barjami found the appropriate range of heating frequencies by scanning a range of frequencies. When ωT_{ac} vs ω is plotted on a log-log scale, the frequency-independent range appears as a plateau, where the frequency is much greater than the internal time constant and much smaller than the external time constant, so the conditions of Eq 2.24 are satisfied.

Original calorimeter design

The existing calorimeter was designed and constructed by Dr Saimir Barjami for his dissertation, under the supervision and guidance of Dr Germano Iannacchione. There

was a single matching network with a resonant frequency of 7.0946×10^6 rad/s, which when connected to the cell results in a natural frequency of 5.056×10^6 rad/s. The calorimeter was used to examine phase transitions of octylcyanobiphenyl with aerosol dispersions of SiO_2.

Heating and Thermometry Design

The RF/MC calorimeter consists of an energy source and an energy dissipation circuit, connected with a waveguide system designed to provide maximal power throughput to the sample, at the chosen frequency. The tuning network is necessary, because when a high frequency electrical signal is transmitted across a transmission line to a load, some energy is absorbed and some is reflected. The tuning network is designed to maximize the energy absorbed while minimizing the reflected energy. The power source is electronically controlled and transmits a sinusoidal signal, which can be modulated at low frequencies. The load consists of the sample, thermistors, and the capacitor plates. For this project, the energy source and the capacitor circuit were left unchanged, while the tuning network was replaced.

The calorimeter was designed to use liquid samples, so the capacitor design was a so-called Cup and Lid design, where there is a plane with a small indentation where the sample is placed, which is sealed with a lid. Because these are the plates of the capacitor, a plastic sheet was used to separate them, eliminating the possibility of electrical shorts. The cup and lid were made using 99.95% pure 0.1mm silver foil, and the plastic sheet is 20x20mm. A Microbead thermistor with a diameter of 0.254 mm and a mass of 0.00001 mg is attached to the cup. Dr. Barjami chose this capacitor design for the following reasons:

1. Good sensitivity response in heat capacity measurements of liquid crystals
2. Good frequency scan response, which is important in minimizing the errors of heat capacity measurements
3. Ease in construction and handling

In order to modulate the temperature, the capacitor is placed in a bath with precise temperature control. The bath is a massive brass cylinder, with walls 2.5cm in thickness,

and a cylindrical cavity 5cm in height and 4 cm in diameter. A heating device is attached to the outside wall of the brass block, with a thermistor in between. Both the thermistor and the heating device are connected to a Lakeshore 340 temperature controller, which provides temperature control. Dr. Barjami found a temperature stability of +/-1 mK over a 30 minute interval at the rim of the brass cylinder, and around 100 μK inside the cavity, which is due to the damping from the massive brass block.

The cylinder is placed in a water bath inside a steel can, which is monitored by another thermometer. In the time since Dr. Barjami published his dissertation, an additional shielding unit has been placed around the calorimeter, providing additional shielding from ambient temperature effects.

Electronic Control Circuitry

The power source consists of several electronic devices, controlled by a computer. A DS345 programmable wave form generator supplies the high frequency signal to the tuning circuit. This generator receives an Amplitude Modulated input from a DS335 function generator, which modulates the high frequency signal with a frequency typical of AC calorimetry, in this case at 15mHz. The DS335 also triggers the digital multimeter, a Keithley Model 2002, to make measurements of the thermistor attached to the capacitor and of the thermometer in the cavity of the brass block. A Lakeshore model 340 controls the temperature at the rim of the brass block, through the heater and thermometer attached to the outside.

The Lakeshore 340, the DS345, the DS335 and the Keithley DMM are all connected to a personal computer, which has been upgraded from Windows 98 to Windows XP. The controller program was written by Dr. Barjami in C++ and compiled under Borland C++, in a multithreaded fashion. One thread controls data acquisition, calculations and printing to disk, while the other controls the temperature. The first thread runs as follows:

1. The function generator DS345 is instructed to output a high frequency signal with an amplitude determined from a .ini file.
2. The DS335 is instructed to output a low frequency (15mHz) signal to the DS345, to modulate the amplitude of the carrier frequency.

3. The program checks with the temperature control thread to determine if the desired temperature has been reached, and waits until it has.
4. The Keithley DMM is told to record the bath temperature T_b, then begin to digitize the bath temperature.
5. The Keithley DMM will digitize the thermistors resistance for 10 periods, or roughly 66.6 seconds.
6. The fitting routine of the received waveform begins, converting the the amplitude of the measured resistance to temperature, and the phase shift between the applied power and resistance to the phase shift between the power and temperature.
7. The Keithley DMM will record the final bath temperature T_a.
8. The heat capacity C* is calculated using (Insert number of Eq 3.10), the phase shift $\varphi = \varphi_{resistance} - \varphi_{power}$, and the bath temperature $T_{PRT} = T_b + T_a / 2$.
9. The program writes the calculated data to disk.
10. The program checks if the temperature control thread signals the end of the temperature scan. If not, it repeats from step 4. If it has, then the program will end.

The temperature control thread runs as follows:

1. Starts the loop that goes through all the zones.
2. Equilibrates the temperature at the starting point of the zone. Signals the main thread.
3. Controls the temperature throughout the zone.
4. When the digitizing is done, signals the main thread that the zone has ended, and starts another zone.
5. Repeat until all the zones have been completed.
6. Signal the main thread to end the program.

Chapter 3: Design and Simulation

In this chapter, the design of the LC matching networks is described. First the purpose of the matching networks is explained, to show the reasoning behind increasing the range of driving frequencies. Then, the simulation of operation at a variety of driving frequencies is used to predict the results, using several dielectric models.

Purpose and Design of the matching networks

Although the electronic circuitry has an operating range of 0-30MHz, the original matching network only allows operation at a single frequency of 5.056×10^6. The calorimeter must be run at that resonant frequency to generate enough heating power, because radio frequency waves have relatively low energy. When the RF/MC calorimeter is operated at a frequency other than the resonant frequency, more of the energy is reflected from the capacitive cell, and consequently less energy can be absorbed by the sample to provide heat.

By increasing the range of possible operating frequencies, the RF/MC calorimeter can be used to investigate the possible frequency dependence of the permittivity of samples. Dr. Barjami has found the permittivity of octylcyanobiphenyl to be strongly temperature dependent, but there currently is no way to investigate frequency dependence.

In order to provide an adequate number of options for the operating frequency, six frequencies were chosen from 15KHz to 5 MHz, with two values per decade. As the natural frequency is equal to the inverse of the square root of the product of the inductance and capacitance, the components were chosen by trying to achieve a regular procession of natural frequencies:

L (μH)	C (nF)	Frequency (ω)	Frequency (KHz)
1000	100	$100x10^3$	15.9
370	8.2	$509x10^3$	81
10	100	$1x10^6$	159
56	1	$4.2x10^6$	672
10	1	$10x10^6$	1,591
1	1	$30x10^6$	5,032

Table 3-1: Values of components in the matching networks, with resulting resonant frequencies

Simulation

Due to some difficulties troubleshooting the matching networks, the effects of different resonant frequencies was unable to be directly tested. However, it is possible to simulate the heating power and provide for comparison with future results. In this section, we will make predictions based on two models. We will simulate expected results for a sample with a constant, frequency-independent permittivity, and one that mimics glycerol by decaying with increasing frequency.

Developing permittivity models

Recall from Eq 2.16 that the power delivered by the matching network is dependent upon the geometry of the capacitor, the driving frequency, resonant frequency, driving voltage, and the loss factor and permittivity. The permittivity is defined as:

3.1 $$\varepsilon = K\varepsilon_0$$

Where the constant of proportionality is usually approximated as a positive real number. However, the permittivity can actually be complex:

3.2 $$K = K' + iK''$$

This complex permittivity is intrinsically related to the loss factor tan δ, which in Chapter 2 was defined as the ratio of the currents in phase with and orthogonal to the applied sinusoidal voltage:

3.3 $$\tan\delta = \frac{I_R}{I_C}$$

This loss factor is also equal to the ratio of the permittivities:

3.4 $$\tan\delta = \frac{I_R}{I_C} = \frac{K''}{K'}$$

Both the real and imaginary components of the permittivity can be frequency dependent. In order to simulate the temperature rises, we will choose two models for this dependence. In the first model, we will use the simplest approximation, where the permittivity has no frequency dependence:

3.6 $$K(\omega) = K' + iK''$$

In the second model, we will assume that the loss factor decreases at higher frequencies. This means that the derivative of K"/K' with respect to frequency is negative. Recalling basic calculus:

3.7 $$\frac{d}{dw}\frac{K''(\omega)}{K'(\omega)} = \frac{K'(\omega)\dot{K}''(\omega) - \dot{K}'(\omega)K''}{K'(\omega)^2}$$

3.8 $$K'(\omega)\dot{K}''(\omega) - \dot{K}'(\omega)K'' < 0$$

3.9 $$K'(\omega)\dot{K}''(\omega) < \dot{K}'(\omega)K''$$

There is a model developed by Debye that will fit this assumption. It is:

3.10 $$K' = \frac{\varepsilon_0 - \varepsilon_\infty}{1+\omega^2\tau^2} + \varepsilon_\infty \text{ and } K'' = \frac{(\varepsilon_0 - \varepsilon_\infty)\omega\tau}{1+\omega^2\tau^2}$$

Where ε_0 is the static permittivity, ε_∞ is the permittivity at very high frequencies, and τ is the relaxation time, which for a dielectric material consisting of spherical molecules in a viscous medium, was shown by Debye to be:

3.11 $$\tau = \frac{4\pi\eta r^3}{kT}$$

where ηis the viscosity of the medium, r is the radius of the spherical molecule, k is the Boltzman constant, and T is the absolute temperature.

To test that this model will fit the assumption, some substitutions will make the math easier to follow:

3.12 Let $K_1 = \frac{K'}{\varepsilon_0 - \varepsilon_\infty}$, $K_2 = \frac{K''}{\varepsilon_0 - \varepsilon_\infty}$, $x = \omega\tau$, and $C = \frac{\varepsilon_\infty}{\varepsilon_0 - \varepsilon_\infty}$

Now Eq. 3.10 becomes:

3.13 $$K_1 = \frac{1}{1+x^2} + C \text{ and } K_2 = \frac{x}{1+x^2}$$

Inserting these equations into Eq. 4.9 gives:

3.14 $$\left(\frac{1}{1+x^2} + C\right)\left(\frac{-x^2+1}{\left(1+x^2\right)^2}\right) < \left(\frac{-2x}{\left(1+x^2\right)^2}\right)\left(\frac{x}{1+x^2}\right)$$

Which simplifies to:

3.15 $$-Cx^4 - Cx^2 + C + 1 < -x^2$$

As x increases, it is trivial to show that this inequality is true given a positive value for C. Therefore, this model will satisfy our original condition: that the loss factor will decrease at higher frequencies.

Simulating the temperature rise

Incorporating the permittivity dependence of the loss factor, the power equation 2.16 becomes:

3.16 $$P = \frac{A}{d}\omega_d \frac{K''}{K'}|\varepsilon| \frac{{V_0}^2}{\left(\left(1-\left(\frac{\omega_d}{\omega_0}\right)^2\right)^2 + \left(\frac{\omega_d}{Q\omega_0}\right)^2\right)}$$

To calculate the temperature rise governed by this power equation, we use the thermal conductances examined in Chapter 3. The temperature rise is given by Ohm's Law, which states that the temperature difference across a thermal resistance due to a heating power P is the product of those two terms:

3.17 $$\Delta T = RP$$

Recalling that a resistance is the inverse of a conductance, we can use the external thermal conductance of the cell enclosing the sample, and the power determined above:

3.18 $$\Delta T = \frac{P(\omega)}{K_e}$$

When the geometry of the capacitor and the driving voltage is fixed, the temperature rise is then governed by the complex permittivity, the driving frequency, and the resonant frequency. When the driving frequency is set to the resonant frequency, the heating power will be maximal, and will be a function of the complex permittivity and the

frequency. As the driving frequency leaves the neighborhood of the resonant frequency, the power will drop off.

In using Eq. 3.16 and Eq. 3.10 to model the heating power, the following values were used for the various constants:

Constant	Value	Constant (for glycerol)	Value
A	1 cm^2	ε_0	44.1
d	2 mm	ε_∞	4.3
V_0	5 V	r	2 nm
Q	80	η	1.5 kg/m s

Table 3-2: values of constants used to model heating power

These values were entered into a spreadsheet designed to allow for easy alteration of any of the assorted variables and constants. Six runs each on the two models were simulated, each centered around one of the resonant frequencies provided by a matching network. Additionally, tests were run by holding the resonant frequency constant and investigating the affects of varying the quality of the circuit. The graphs of heating power as a function of frequency looked as expected, with a peak at the resonant frequency, falling away above and below the resonant frequency.

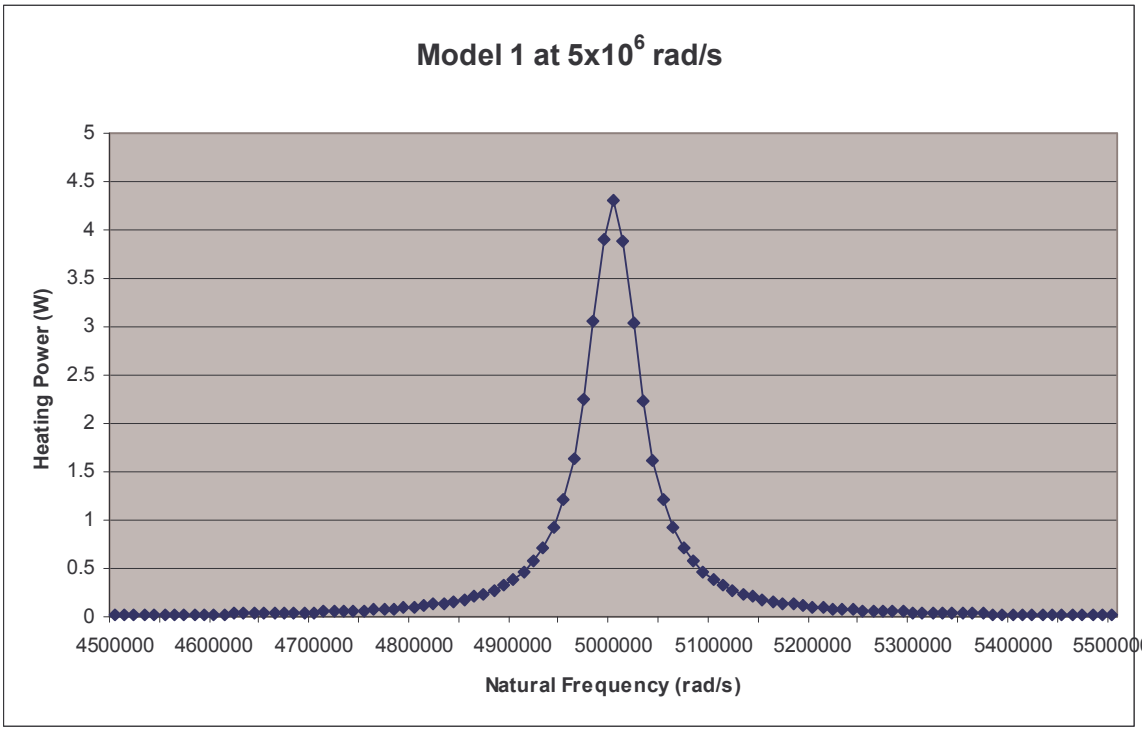

Figure 3-1: Constant-permittivity model at $5x10^6$ rad/s

Figure 3-1 shows the behavior of the constant-permittivity model, with a well-defined peak and attenuating above and below resonance. When the decreasing-permittivity model was graphed, the outcome was similar.

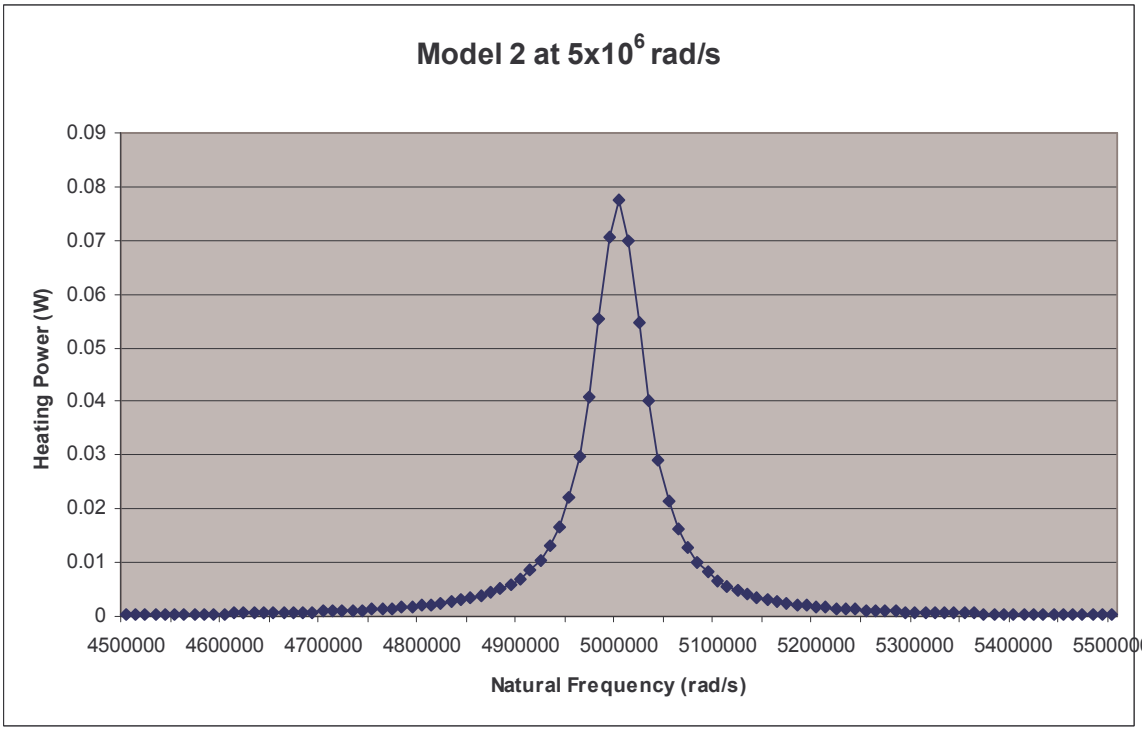

Figure 3-2: Decreasing-permittivity model at $5x10^6$ rad/s

Figure 3-2 shows that while the curve looks qualitatively similar to the constant-permittivity model, the peak power at resonance is significantly lower. When a table is compiled of the peak power at different resonant frequencies, it becomes clear that permittivity strongly affects the heating power.

Frequency(rad/s)	Model 1 Power (W)	Model 2 Power (W)
100000	0.086000358	0.125836799
500000	0.430001791	0.086080692
1000000	0.860003582	0.079800752
5000000	4.300017908	0.077532439
10000000	8.600035817	0.07745924
30000000	25.80010745	0.077437523

Table 3-3: Peak power at different resonances

When the circuit is run at the resonant frequency, Eq. 3.16 simplifies to:

3.18 $$P = \frac{A}{d}\omega_0 \frac{K''}{K'}|\varepsilon|Q^2 V_0^2$$

It is immediately obvious that given constant permittivity, the power scales with the resonant frequency, which is shown in Table 3-3. However, if the permittivity decreases with increasing frequency, this is not true, and given these particular values for static and high-frequency permittivities, the power actually decreases at higher frequencies. This will affect the decision of what resonant frequency is desired for a given sample and its permittivity characteristics.

The quality of the overall circuit also has a strong affect on the peak heating power, as well as on the shape of the curve.

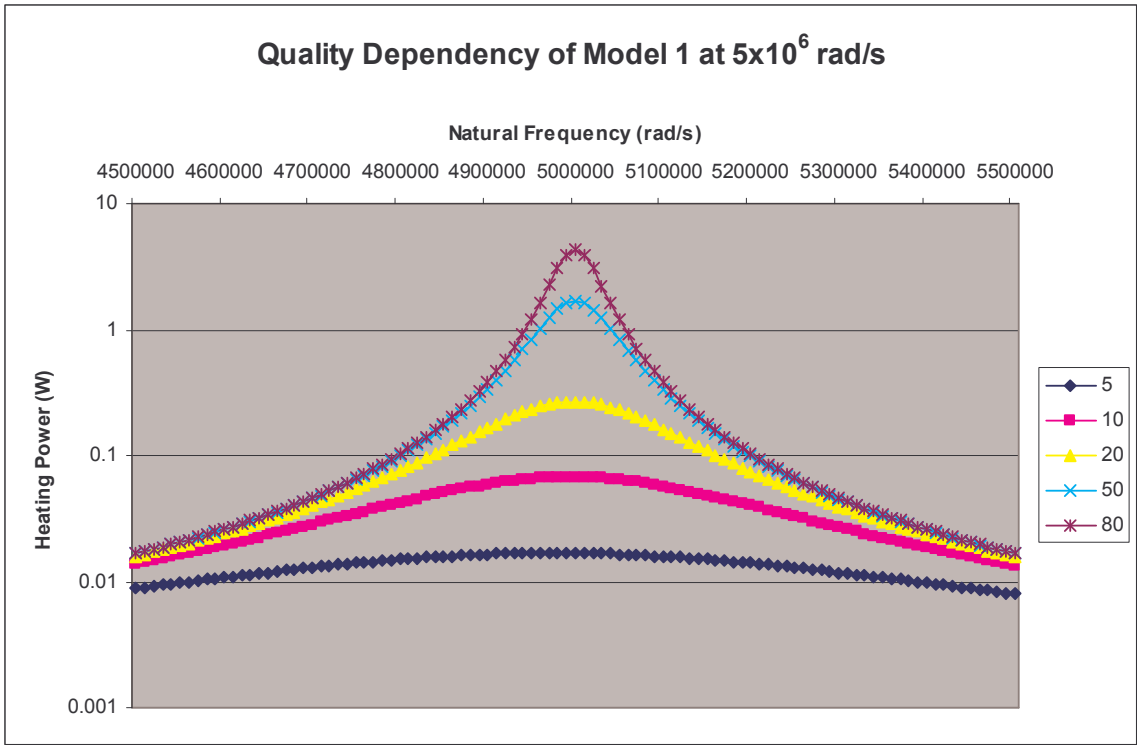

Figure 3-3: Quality Dependency of Constant-Permittivity model at $5x10^6$ rad/s

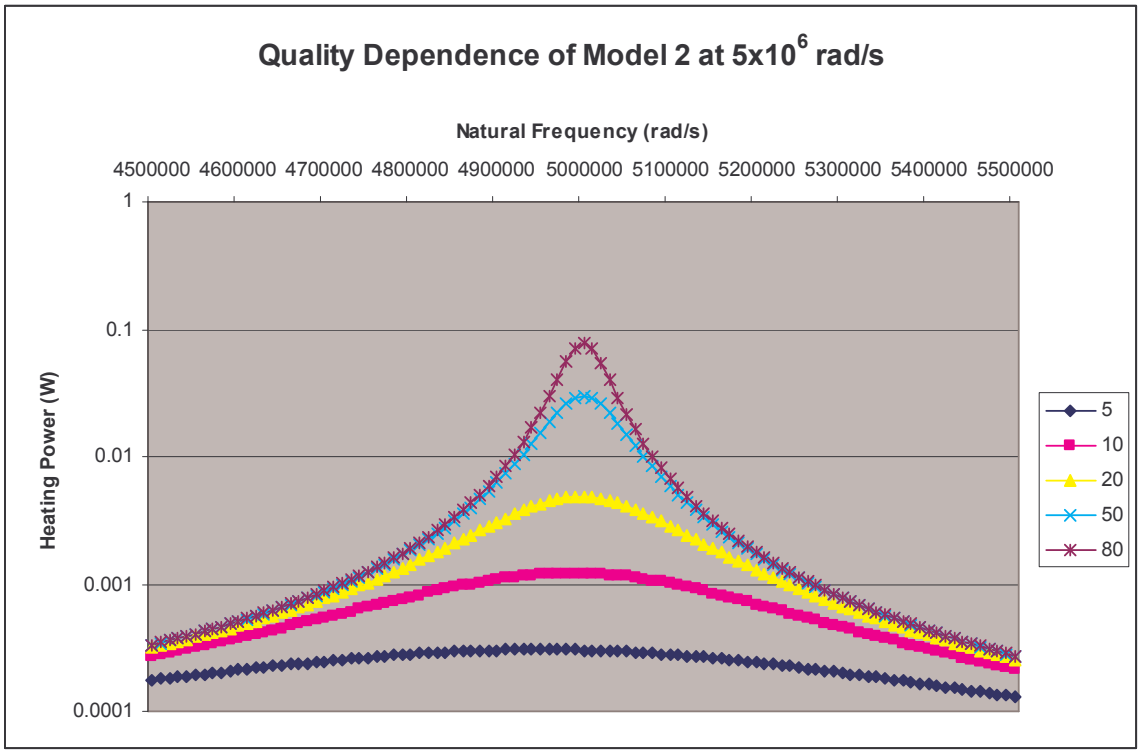

Figure 3-4: Quality Dependency of Decreasing-Permittivity model at $5x10^6$ rad/s

Figures 3-3 and 3-4 show what happens to the models when the quality is varied, on a logarithmic scale. At a low quality, the peak is smoothed out, and it is less

important to run exactly at resonance, although the peak is also lower, which is not desirable when wanting to be able to rapidly heat a sample. As the quality increases, the peak gets higher and more pronounced, as is to be expected. Again, at all qualities the constant-permittivity model has a higher value than the decreasing-permittivity model.

Chapter 4: Conclusions and Recommendations for Future Research

In developing this model for the heating power of RF Calorimetry, several conclusions were developed, with both expected and unexpected results. The graphs of heating power around resonant frequency were as expected from prior research and similarity to other physical systems. Although it was expected that the heating power would depend upon the permittivity, the behavior that developed was different from expectations. From the results of this project, several suggestions for future work are provided, both experimental and theoretical.

Conclusions

Prior to the beginning of simulation, there were firm expectations of the qualitative behavior of heating at frequencies near resonance. These expectations were built from the prior work of Dr Barjami, as well as due to the fact that the circuit is in essence a driven damped oscillator, and should show behavior similar to other physical systems such as a driven pendulum or vibrating spring. It was expected that there would be a peak output at resonance, falling off rapidly as the frequency moved away from resonance. As this behavior was confirmed in the simulation, there is a high level of confidence in the ability of this model to simulate RF Calorimetry.

There were no such prior expectations as to the quantitative behavior of the heating power absorbed by a sample with a frequency-dependent permittivity, and the results provided original insight into how best to investigate such materials with the RF Calorimeter. The heating power is strongly dependent upon resonant frequency, and decreases at higher frequency. Therefore, materials with a similar frequency-dependent permittivity are best studied at relatively low frequencies, to maximize the heating power.

Directions of future work

This project has opened up directions for future research that previously would not have been seen as interesting, due to the new insights on how permittivity affects the heating power. Future research could include additional permittivity models,

investigation of the dependence of the permittivity on the heating power, and lastly, pushing the limits higher and lower for the resonant frequency.

The scope of this project included two models of permittivity, but more could be added. The addition of increasing-permittivity models or non-monotonic models would be insightful, to see how that would affect the heating power at different resonant frequencies. Theoretically, there could be a permittivity model that behaves such that the peak heating power is not at resonance, due to local minima or maxima of the permittivity in the neighborhood of the resonant frequency.

Complementary to the addition of other permittivity models, more mathematical investigation of how permittivity affects the heating power could be done. This would be very straightforward, as the heating power is either directly or inversely proportional to the imaginary permittivity, the real permittivity, and the absolute permittivity. This investigation could be used to guide what sort of permittivity models would produce interesting results.

More research could also be done on the upper and lower limits of frequency. This project focused on frequencies immediately obtainable by the specific RF Calorimeter in the lab of Dr Iannacchione, but it could be illuminating to investigate the static and high-frequency limits. The current results suggest that at constant permittivity, higher resonant frequencies always produce higher heating powers, and the inverse for decreasing-permittivity models. However, physical effects that were not simulated will certainly provide constraints, and it would be useful to know the domain over which this simulation is realistic.